Journal of Colloid and Interface Science 552 (2019) 781–793

Contents lists available at ScienceDirect

Journal of Colloid and Interface Science

journal homepage: www.elsevier.com/locate/jcis

Regular Article

Structural parameters of soft PNIPAM microgel particles as a function of crosslink density

Suhad Sbeih [a,b], Priti S. Mohanty [c], Michael R. Morrow [a,*], Anand Yethiraj [a,*]

[a] Department of Physics & Physical Oceanography, Memorial University, St. John's, Newfoundland Labrador A1B3X7, Canada
[b] School of Basic Sciences and Humanities, German Jordanian University, Amman, Jordan
[c] School of Chemical Technology, Kalinga Institute of Industrial Technology (KIIT) Deemed to be University, Bhubaneswar 751024, India

GRAPHICAL ABSTRACT

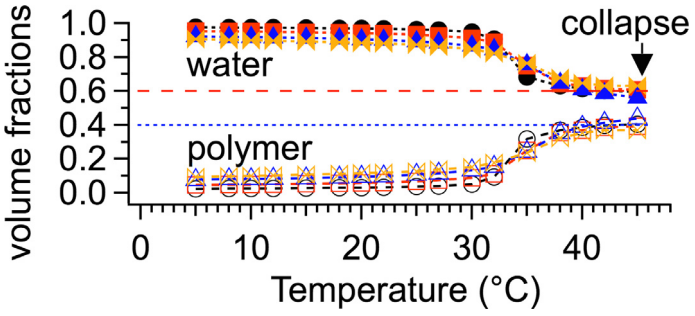

ARTICLE INFO

Article history:
Received 12 October 2018
Revised 14 May 2019
Accepted 15 May 2019
Available online 22 May 2019

Keywords:
Colloid
Microgel
Structure
Swelling
Rheology
Water content

ABSTRACT

Hypothesis: The temperature dependences of hydrodynamic radii in thermo-sensitive microgel suspensions, known as collapse curves, are commonly fitted to the benchmark Flory-Rehner theory but parameters obtained often yield little physical insights. Our study of poly(N-isopropylacrylamide) (PNIPAM) microgel suspensions in water is driven by the hypothesis that fitting to Flory-Rehner theory can yield meaningful parameters that separate into ones that are insensitive to crosslink density or deuteration and ones that are not.

Experiments: Dynamic light scattering (DLS) and rheology experiments were done on 8 microgel variants, protonated and deuterated PNIPAM for four crosslink densities, synthesized under otherwise identical conditions.

Findings: Remarkably, polymer volume fractions in the microgel particle at collapse, $\phi_{collapse}$, obtained via rheology, are independent of crosslink density. Along with collapse curves from DLS, this determines the temperature dependence of microgel water and polymer volume fractions. Fitting collapse curves to Flory-Rehner theory yields reference polymer volume fractions, ϕ_0, associated with microgel particle elasticity. ϕ_0 is much lower than $\phi_{collapse}$, and increases with crosslink density. For all microgel sample variants, a crossover temperature, where the elastic contribution to osmotic pressure changes sign, is found to approximate the final temperature after microgel synthesis and also to the free polymer θ temperature.

* Corresponding authors.
E-mail addresses: mmorrow@mun.ca (M.R. Morrow), ayethiraj@mun.ca (A. Yethiraj).

https://doi.org/10.1016/j.jcis.2019.05.047
0021-9797/

1. Introduction

Colloidal suspensions have been used very successfully as model systems to understand the fundamentals of phase transitions in condensed matter [1–6]. Colloidal interactions, including tunable interactions [7–9], that are "soft" in the sense of being describable by longer-ranged interaction forces than the hard-sphere interaction, are crucial to accessing information about phase transition kinetics. Among systems that exhibit multiple modes of tunability are colloidal microgels.

Microgel colloidal suspensions, such as poly(N-isopropylacrylamide) (or PNIPAM) in water, are aqueous polymer solutions that are intermediate between branched polymers and macroscopically crosslinked systems [10,11]. It is, however, very productive to think of them as "soft" colloidal suspensions [12,13]. They can be uncharged [12] or charged [14], with a hydrodynamic size that is sensitive, as highlighted in a recent review [15], not only to temperature, pH, ionic strength, and concentration, but also pressure [16] and external electric fields [17].

While the macroscopic properties of microgel colloidal suspensions has been studied extensively in the last two decades (see, for example, a recent review [18]) and can have rich phase behavior [19,14], the internal structure and dynamics remains a question of active interest [20–24], especially their dependences on crosslink density [25]. There has been a renewed interest in achieving a quantitative understanding of the microgel swelling-deswelling behavior as a function of temperature [26–29]. In particular, it has been noted [28] that a gel-swelling theory such as the classic Flory-Rehner theory, originally developed to describe rubber elasticity [30], presents a challenge: it is hard to infer much from fits of experimental swelling curves to theory because of the number of fit parameters (seven in total) available to match the experimental monotonic decrease of hydrodynamic radius as a function of temperature.

We were motivated to begin the current study in order to study the internal microscopic dynamics of microgels as a function of crosslink density by deuterium NMR, using deuterated PNIPAM while studying macroscopic dynamics *via* rheology and dynamic light scattering. We found, however, that using both protonated and deuterated PNIPAM, and employing the techniques of rheology and DLS, we could also achieve robust fits with a reduced set of free parameters, and make definitive statements about water and polymer content of microgel particles as a function of temperature, as well as evaluating key gel-swelling parameters in the context of Flory-Rehner theory. This is the focus of the current work.

2. Background

2.1. Dynamic light scattering and Flory-Rehner phenomenology

Gel-swelling theories [26,27,31] such as the classic Flory-Rehner theory write down the elastic and mixing contributions to the osmotic pressure Π, and set the total osmotic pressure to zero in order to obtain an expression for the temperature dependence of the either the particle size R_H or, equivalently, the polymer volume fraction, ϕ, in each microgel "particle", using the relation

$$\phi = \phi_{\text{collapse}}\left(\frac{R_{\text{collapse}}}{R_H}\right)^3, \tag{1}$$

where R_{collapse} and ϕ_{collapse} are reference polymer hydrodynamic radius and polymer volume fraction in the collapsed state. ϕ is sensitive to environmental conditions such as temperature T, pH, and microgel concentration C.

The mixing contribution to the osmotic pressure [25,28,32] is

$$\frac{\Pi_{\text{mix}}}{k_BT} = \frac{N_A}{\nu_{\text{molar}}}\left[\phi + \ln(1-\phi) + \chi\phi^2\right], \tag{2}$$

where N_A is the Avogadro number, ν_{molar} is the molar volume of the solvent, and χ is the Flory–Huggins solubility parameter. While χ typically has an explicit temperature dependence, in the microgel literature it is found that one needs to add a phenomenological ϕ dependence in order to fit data. The form that has been used for χ is

$$\chi = 0.5 - A(1-\theta/T) + C\phi + D\phi^2 \tag{3}$$

where A is related to the second virial coefficient and θ is the theta temperature, which can be constrained to the linear polymer value. C and D are phenomenological fit parameters.

The elastic contribution to the osmotic pressure within the particle is written as

$$\frac{\Pi_{\text{el}}}{k_BT} = \frac{N_{\text{chain}}}{V_0}\left[0.5\frac{\phi}{\phi_0} - \left(\frac{\phi}{\phi_0}\right)^{1/3}\right], \tag{4}$$

where N_{chain} is the number of polymer chains in the network (in each microgel particle) and V_0 and ϕ_0 are the volume and polymer volume fraction of the microgels in the reference state. The reference state was originally thought to be the preparation state where the crosslinking was performed because any deviation from that state would induce elastic stress on the polymer network. [30] The microgel synthesis is carried out at 70 °C. At this temperature, the polymer is in the collapsed state, and it would be reasonable to equate ϕ_0 and ϕ_{collapse}. However, the reaction is completed while the synthesis mixture is stirring and cooling back to room temperature. It is thus unclear what ϕ_0 should be.

Indeed, as discussed in a recent review of gel swelling theories [26], "this reference state is not well-defined for gels prepared in the presence of solvent, and its determination is still a controversial issue". Lopez and Richtering [28] showed, convincingly, that it is preferrable to implement fits of Flory-Rehner theory to experimental results *without* assuming that $\phi_0 = \phi_{\text{collapse}}$, and by limiting parameter values as much as possible. Moreover, the parameters A, C, and D in Eq. 3 should typically be of order unity. This is the philosophy adopted here. Thus, in terms of the hydrodynamic radius measured by DLS, as a function of temperature T, the (by now, semi-phenomenological) Flory–Rehner fit equation is

$$T = \frac{-A\phi^2\theta}{\phi + \ln(1-\phi) + (0.5-A)\phi^2 + C\phi^3 + D\phi^4 + \frac{N_{\text{chain}}\nu_{\text{molar}}}{V_0N_A}\left[0.5\frac{\phi}{\phi_0} - \left(\frac{\phi}{\phi_0}\right)^{1/3}\right]}, \tag{5}$$

coupled with Eq. 1 for ϕ. In Eq. 5, we further use, following Lopez and Richtering the relation $\frac{N_{\text{chain}}\nu_{\text{molar}}}{V_0N_A} \approx 0.35\phi_0 f$, where f is the molar fraction of crosslinker which is related to crosslinker to monomer weight ratios, m_{BIS}/m_{NIPAM}, that are controlled at synthesis (see Section 3.1).

2.2. Relating the "watery colloid" to microgel rheology

In a suspension of reference volume V, there are N microgel (colloidal) particles. An isolated microgel particle suspended in water consists of only PNIPAM polymer and water, thus $V = V_{\text{particle}} + V_{\text{medium}}$, where V_{particle} is the total microgel particle volume and V_{medium} is the total "medium" volume: this refers to only the water outside the particle. The microgel particle volume fraction can be defined as

$$\Phi_c = \frac{V_{\text{particle}}}{V_{\text{particle}} + V_{\text{medium}}} = \frac{1}{1 + \frac{V_{\text{medium}}}{V_{\text{particle}}}}. \tag{6}$$

The total volume of water in the system (inside and outside the particle) is independent of temperature and given by

$V_w = V_{\text{medium}} + \phi_w V_{\text{particle}}$, where ϕ_w, the fraction of the colloidal particle volume accounted for by water, is temperature dependent. From this relation, one can say that the volume of the particle-bound water is $\phi_w V_{\text{particle}}$. The PNIPAM volume per particle in the system is presumed to be independent of temperature, and can be defined as a factor v_{polymer} such that

$$v_{\text{polymer}} = \frac{V_{PNIPAM}}{N} = (1-\phi_w)\,\frac{V_{\text{particle}}}{N}, \tag{7}$$

where N is the total number of colloidal particles in the reference volume V. This last identification is true even with particle overlap, because V_{PNIPAM} is the *total* polymer volume. In Eq. (7), both the total colloidal particle volume V_{particle} and the particle-bound water fraction depend on temperature. Dividing the total water volume in the system by the PNIPAM volume in the system gives

$$\frac{V_w}{V_{PNIPAM}} = \frac{\frac{V_{\text{medium}}}{V_{\text{particle}}} + \phi_w}{1-\phi_w}.$$

The ratio of solvent volume to particle volume can then be written as

$$\frac{V_{\text{medium}}}{V_{\text{particle}}} = \left[\frac{V_w}{V_{PNIPAM}}(1-\phi_w)\right] - \phi_w. \tag{8}$$

The concentration by weight of the sample is $C = m_{PNIPAM}/(m_{PNIPAM} + m_w)$, where m_{PNIPAM} and m_w are the experimentally measured masses of PNIPAM powder and water. The densities of PNIPAM and water are known and they have the values $\rho_{PNIPAM} = 1.1\ \text{g/cm}^3$ and $\rho_w = 1\ \text{g/cm}^3$. By converting masses to density-volume products in the previous equation and rearranging, we get $V_w/V_{PNIPAM} = (\frac{1}{C} - 1)(\rho_{PNIPAM}/\rho_w)$. The particle volume fraction now can be expressed in terms of ϕ_w, C, ρ_{PNIPAM}, and ρ_w by substituting the concentration-dependent form of V_w/V_{PNIPAM}, above, into Eq. (8), and substituting the result into Eq. 6. The equation for the microgel particle volume fraction then becomes

$$\Phi_c = \frac{1}{(1-\phi_w)\left[1 + \left(\frac{1}{C} - 1\right)\frac{\rho_{PNIPAM}}{\rho_w}\right]}. \tag{9}$$

The $(1-\phi_w)$ factor can be replaced by the ratio of $\frac{N v_{\text{polymer}}}{V_{\text{particle}}} = \frac{v_{\text{polymer}}}{v_{\text{particle}}}$, using Eq. 7, where we have defined a single particle volume $v_{\text{particle}} = V_{\text{particle}}/N$. The quantity $v_{\text{polymer}}/v_{\text{particle}}$ is the polymer volume fraction ϕ that was used in Section 2.1, so consistently, $\phi = 1 - \phi_w$. The single-particle volume, v_{particle}, only equals $\frac{4}{3}\pi R_H^3$ (obtained from DLS) in the absence of overlap. Using these definitions, the microgel particle volume fraction can be expressed as [33]

$$\Phi_c = \frac{v_{\text{particle}}}{v_{\text{polymer}}\left[1 + \left(\frac{1}{C} - 1\right)\frac{\rho_{PNIPAM}}{\rho_w}\right]}. \tag{10}$$

It should be noted that, when the concentration $C \ll 1$, this reduces to $\Phi_c \approx \left(\frac{v_{\text{particle}}}{v_{\text{polymer}}}\right)\left(\frac{\rho_w}{\rho_{\text{PNIPAM}}}\right)C \sim kC$. This is the form typically employed in the literature, but Eq. 10 is the more correct form. In the collapsed phase, it is reasonable to assume that the viscosity of a *dilute* microgel suspension behaves like that of an effective hard sphere suspension. The relative viscosity $\eta_{rel} = \eta_0/\eta_s$ (where η_0 is the zero-shear viscosity of the suspension and η_s is the viscosity of the solvent, i.e., water at the same temperature) can be fit to the phenomenological Krieger-Dougherty equation [34] for hard spheres, $\eta_{rel} = (1 - \Phi_c/\Phi_c^*)^{-2.5\Phi_c^*}$, where $\Phi_c^* = 0.63$ is the packing fraction at which the relative viscosity of hard spheres goes to infinity [35], and is close to the $\Phi_{rcp} = 0.64$ maximum packing fraction for a random packing of hard spheres. In the present work, this hard-sphere equation is simply inverted to obtain the colloidal suspension packing fraction Φ_c from a measured relative viscosity η_{rel},

$$\Phi_c = \Phi_c^*\left[1 - \eta_{rel}^{1/(-2.5\Phi_c^*)}\right], \tag{11}$$

to obtain an estimate of the volume fraction in this temperature range. Using Eqs. (10) and (11), we then obtain

$$\phi \equiv \frac{v_{\text{polymer}}}{v_{\text{particle}}} = \frac{1}{\Phi_c^*\left[1 - \eta_{rel}^{1/(-2.5\phi_c^*)}\right]\left(1 + \left(\frac{1}{C} - 1\right)\frac{\rho_{PNIPAM}}{\rho_w}\right)}. \tag{12}$$

The left hand side of Eq. 12 is the polymer volume fraction ϕ inside the microgel particle. The water fraction is $\phi_w = 1 - v_{\text{polymer}}/v_{\text{particle}}$. The right hand side of Eq. 12 consists of the microgel concentration C, which is controlled, the density of PNIPAM and water, which are known, and η_{rel}, which is obtainable *via* fits to microgel rheology experiments.

2.3. Viscosity and the cross equation

The Cross equation [36] describes a range of shear-thinning behavior in gels, and is commonly used as a phenomenological model to describe shear-rate dependent viscosities in microgel particles [12,37,38]. The characteristic features of the Cross equation,

$$\eta - \eta_\infty = \frac{\eta_0 - \eta_\infty}{1 + (\tau\dot{\gamma})^m}, \tag{13}$$

are a limiting ("zero-shear") viscosity, η_0, at very small shear rates, a limiting viscosity at very high shear rates, η_∞, a power-law shear-thinning regime (with exponent m) and a characteristic timescale τ, which is the inverse of the shear rate required for onset of the power law regime.

3. Experimental

3.1. Microgel synthesis

An example of microgel synthesis, following the procedures laid out by by Senff and Richtering [12], is given below. First, 0.997 g of the d3 NIPAM monomer (> 98% purity) and 0.0752 g of crosslinker BIS (N,N′-methylenebis(acrylamide), 99% purity) were dissolved in 80 ml of distilled water (the uncertainty in measured masses was ±0.0005 g). Separately, 0.0235 g of SDS (sodium dodecyl sulfate, 98.5+% purity) surfactant was dissolved in 10 ml water. Non-deuterated monomer (h-NIPAM, 97% purity) crosslinker BIS, initiator KPS (potassum persulfate, ⩾ 98% purity), and surfactant SDS were obtained from Sigma Aldrich Inc., Oakville, ON, Canada. Deuterated monomer was obtained from Polymer Source Inc., Dorval, QC, Canada. The mixtures were transferred into a 250 ml round-bottom flask. The mixtures were heated at 70 °C and degassed under a gentle nitrogen stream with a stirring speed of 270 rpm for 45 min. Finally, 0.0363 g of the initiator, KPS, dissolved in 10 g of water, was added slowly to initiate the polymerization. The reaction mixture was kept at 70 °C under gentle nitrogen gas flow for 6 h to complete the reaction with a heater stirring speed of 270 rpm. The reaction was stopped after 6 h by switching off the heater. The stirring was maintained while the sample cooled back to room temperature, and then continued overnight to keep the particles from being trapped in the collapsed state after the high temperature synthesis.

After synthesis, the microgel suspension was purified in order to remove un-reacted monomers and ionic impurities. First the product of the synthesis was centrifuged using an ultracentrifuge at 40,000–50,000 rpm for 45–60 min to sediment the microgel particles. This centrifugation was carried out at 35 °C to ensure that particles were in the higher density collapsed phase. After centrifugation, the supernatant was removed and the remaining microgel suspension was diluted with deionized water and redispersed by

vortex and ultrasonication cycles. With the ultrasonic bath set at 30 °C, the diluted suspension was ultrasonicated for about 2 h in total with additional vortexing for 1–2 min every 15 min. Following redispersion, the sample was centrifuged again. This part of the procedure was carried out 6 times in order to remove unreacted monomers. After this, the purified microgel suspensions were dialyzed against deionized water for one week. Once the microgel suspension was purified, the swelling transition (i.e. temperature dependence of hydrodynamic radius) was characterized using dynamic light scattering at dilute concentration. Finally, the microgel suspensions were freeze dried and kept for future use.

This process was carried with h-NIPAM and d3-NIPAM and for four different crosslinker-to-monomer ratios m_{BIS}/m_{NIPAM}. This ratio can be related to the "crosslink density" (or more precisely, the crosslinker molar fraction) f via $f^{-1} = 1 + \frac{M_{W,BIS}}{M_{W,NIPAM}} \frac{m_{NIPAM}}{m_{BIS}}$, with $M_{W,BIS} = 154.17$ g/mole, while $M_{W,NIPAM}$ is 113.16 g/mole and 116 g/mole, respectively, for h- and d3-NIPAM. In the example synthesis above, $m_{BIS}/m_{NIPAM} = 0.0754 \sim 7.5$ wt%, corresponding to $f = 0.0524$. A nearly identical synthesis for d3-NIPAM gave $f = 0.0537$. We thus use the value $f = 0.053 \pm 0.001$ for these syntheses of h- and d3-NIPAM. Average cross-link densities were similarly calculated for protonated and deuterated samples synthesized at other crosslinker-to-monomer mass ratios.

3.2. Dynamic light scattering

Dynamical light scattering (DLS) was carried out on a Zetasizer Nano ZS (Malvern Instruments, Montreal, QC, Canada), which uses a 633 nm He-Ne laser and a detector in a back-scattering geometry (173°). DLS experiments were carried out in dilute suspensions (0.04 wt%) and in deionized water. Measurements were carried out from 5 to 45 °C with 2–3 °C steps. The hydrodynamic radius R_H of the microgel particle as a function of temperature was obtained from the DLS measurements. The mean hydrodynamic radius, R_H, and its standard deviation were obtained from the autocorrelation functions using the inbuilt software which applies a cumulants analysis, i.e.,a nonlinear least squares fit of a polynomial to the natural log of the autocorrelation function. The accuracy of the obtained radii was cross-checked in test samples by direct fitting of the raw autocorrelation functions. We verified the unimodal character of all suspensions studied.

3.3. Rheology

The dynamic viscosity was measured using a Anton Paar Physica MCR 301 strain-controlled rheometer (Anton Paar Inc., Montreal, QC, Canada) using the cone-plate CP50-1 configuration with a 50 mm diameter and a 1° cone angle.

Samples for rheology were prepared using only the protonated microgel powders and de-ionized water. After adding water to powder, the mixture was stirred for 2 min and then placed in an ultrasonic bath for 2 h. For each crosslink density, suspensions were prepared at a range of concentrations from 1 to 12 wt%. A sample quantity of approximately 600 µl was loaded into the cone-plate system. Every experiment was preceded by testing of a water sample for calibration. The measurements were carried out from a shear rate $\dot{\gamma}$ of 10^{-2} or 10^{-1} s^{-1} to a value of 10^4 s^{-1}. Each measurement was preceded by pre-shear at 5 s^{-1} of 0.5–1 min, and a waiting time of 1 min. The measurements were typically repeated 3 times to check for steady-state behavior.

4. Results and discussion

The temperature dependence of the hydrodynamic radius, R_H, for both non-deuterated ("h") and deuterated ("d3") synthesized PNIPAM microgels is plotted in Fig. 1(a)–(d) for four different crosslink molar fractions ($f = 0.011, 0.053, 0.092, 0.127$). While the absolute particle size is somewhat sensitive to synthesis conditions (such as surfactant concentration), the h-NIPAM microgel particle (open red symbols) is systematically larger in Fig. 1(a-d) than the d3-NIPAM microgel (solid blue symbols). Using the particle *volume* at 45 °C as reference, one can calculate a temperature-dependent swelling factor

$$S(T) = \left(\frac{R_H(T°C)}{R_H(45°C)}\right)^3, \tag{14}$$

which in the range of our observations (between 5 and 45 °C) has a maximum value $S_{max} \equiv S(5\,°C)$. The swelling factor S(T) (Fig. 1(e)) shows a systematic decrease with crosslink density f for both protonated and deuterated PNIPAM syntheses, and is indifferent to the particle size at synthesis.

It should be noted that some workers [25] report, instead, a "de-swelling factor" $\beta(T) = (R_H(T_{ref})/R_{swollen})^3$ at a particular reference temperature T_{ref} in the swollen state. Because the R_H vs temperature curve is flatter in the collapsed state (at $T = 45$ °C) than in the swollen state at ($T = 5$ °C), the swelling factor defined above is a bit cleaner, but the two are simply related: $S(T) = \beta(T)S_{max}$. This swelling factor $S(T)$ can be obtained directly from Eq. 14 and the R_H results shown in Fig. 1(a) and (b). It has the largest range for the lowest crosslink density and it is systematically smaller with increasing f. This can be seen by plotting the *maximum* swelling factor S_{max} as a function of f. It is seen (Fig. 1 (e)) that $S_{max} \equiv S(5\,°C)$ decreases roughly linearly from about 15 to 5 with increasing f (symbols). It should be noted that the swelling factors reported in some previous work (e.g. Varga et al. [20]) are given in terms of particle diameter rather than volume, and based on reference low/high temperatures of 25 °C/40 °C rather than the 5 °C/45 °C used in this work. When these differences are accounted for, the results are roughly consistent with those reported here.

We can construct a dimensionless and normalized particle volume increment

$$V_{norm}(T) = (S(T) - 1)/(S_{max} - 1), \tag{15}$$

that is zero at $T = 45$ °C and unity at $T = 5$ °C. One observes (for both h- and d3-PNIPAM) that the temperature dependence of this particle volume increment, $V_{norm}(T)$, collapses onto a single curve in the swollen phase. This is shown in Fig. 2(a) and (b). While identifying a transition temperature for microgel suspensions is often challenging, this data collapse in the swollen phase allows us to unambiguously assign a transition temperature in the region where one first observes deviation from the data collapse. A choice of $V_{norm}(T) = 0.2$ appeared to be a good indicator of the transition temperature at all crosslink densities, and for both protonated (h) and deuterated (d3) PNIPAM. Even if this indicator is somewhat arbitrary, it certainly allows a systematic comparison of transition temperatures between samples at different crosslink densities. As shown in Table 1, with increasing crosslink density, there is a systematic increase in transition temperature for both protonated and deuterated PNIPAM.

It would be interesting to examine the DLS results presented above from the point of view of gel-swelling theories [26,27] such as the classic Flory-Rehner theory. However, it has been pointed out [28] that the results of fits are only meaningful if the parameters are properly constrained. We thus postpone this discussion until after a presentation of rheology results, from which we can independently obtain estimates of the polymer volume fraction $\phi = v_{polymer}/v_{particle}$ inside a microgel particle.

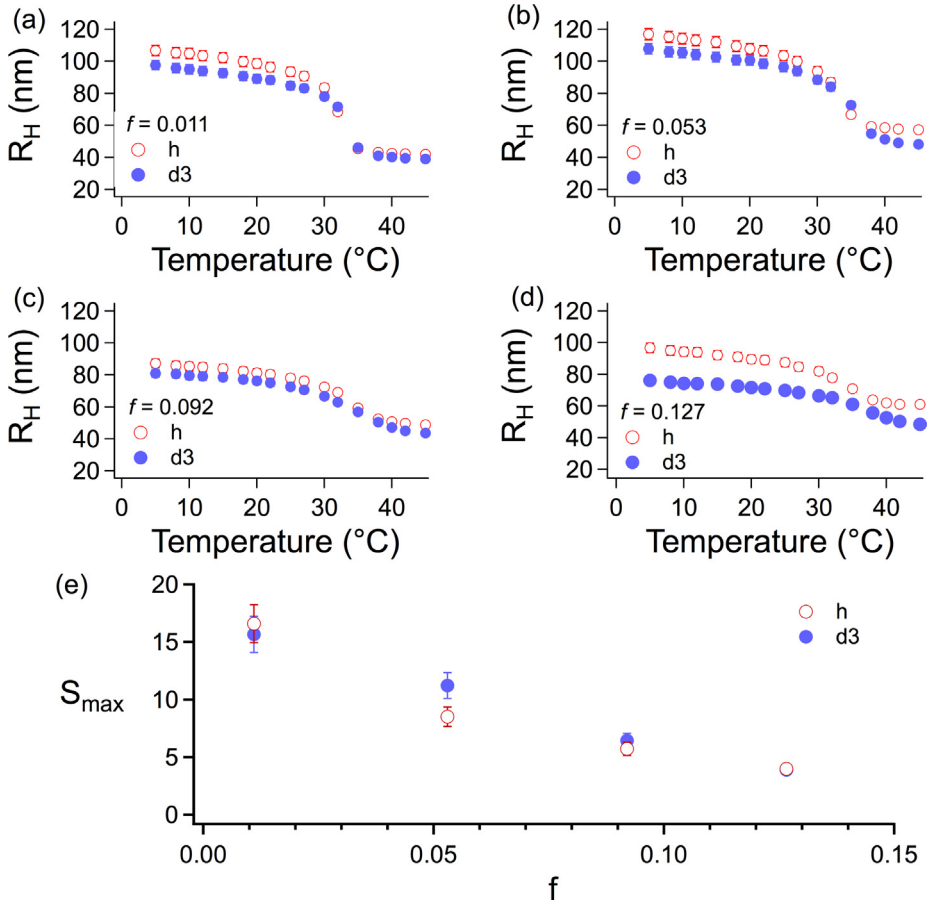

Fig. 1. The hydrodynamic radius R_H as a function of temperature for both the h-PNIPAM (red, open circles) and the d3-PNIPAM (blue, solid circles) syntheses obtained from DLS measurements for four crosslink densities (a) $f = 0.011$ (c) $f = 0.053$ (c) $f = 0.092$ (d) $f = 0.127$. (e) The maximum observed swelling factor (at $T = 5\ ^\circ C$) S_{max} as a function of crosslink molar fraction f for both h- and d3-PNIPAM microgels. (For interpretation of the references to colour in this figure legend, the reader is referred to the web version of this article.)

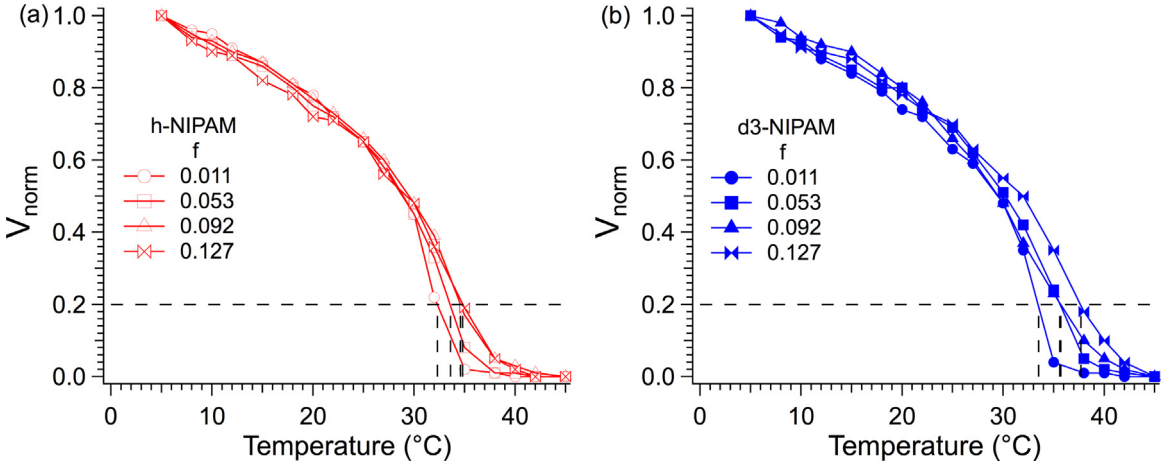

Fig. 2. V_{norm} as a function of temperature for both (a) the h PNIPAM and (b) the d3 PNIPAM syntheses obtained from DLS measurements. The dashed horizontal line at $V_{norm} = 0.2$ was used to find the transition temperature.

4.1. Rheology

Shown in Fig. 3 are the results of steady shear rheology measurements in a microgel suspension at a single crosslink density, $f = 0.092$, and particle concentration, $C = 8$ wt%. Similar experiments were carried out for all crosslink densities, at chosen particle concentrations, of h-PNIPAM suspensions. The viscosity η as a function of shear rate $\dot{\gamma}$ shows a strong non-Newtonian, shear-thinning behaviour at all but the highest temperatures. In the range of shear rates probed ($10^{-2} < \dot{\gamma} < 10^{4}\ s^{-1}$), we observe a low-shear-rate plateau above $T = 20\ ^\circ C$, while for $T < 20\ ^\circ C$ the slopes, on a log–log plot, all seem comparable with no plateau. It

Table 1
The swelling factors, S_{max}, and the transition temperatures, T_{trans}, as function of crosslink density for both non-deuterated (h) and deuterated (d3) microgels. There is a systematic variability of 0.5 °C in the reported transition temperature values upon varying the threshold.

		h-PNIPAM syntheses		d3-PNIPAM syntheses	
m_{BIS}/m_{NIPAM} (wt%)	f	S_{max}	T_{trans} (°C)	S_{max}	T_{trans} (°C)
1.5	0.011	17 (1)	32.3 (1)	16 (1)	33.5 (1)
7.5	0.053	8.5 (8)	33.6 (1)	11 (1)	35.6 (1)
13.6	0.092	5.7 (5)	34.6 (1)	6.4 (6)	35.7 (1)
19.5	0.127	4.0 (4)	34.8 (1)	3.9 (4)	37.7 (1)

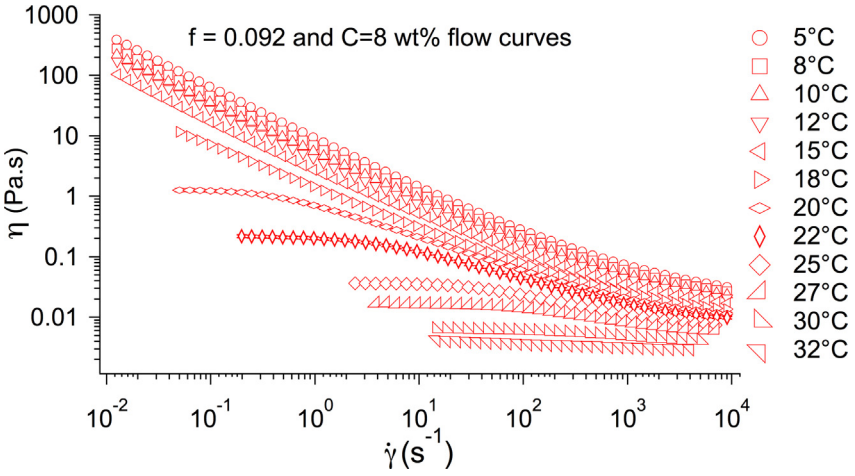

Fig. 3. The viscosity *versus* shear rate at all temperatures for the microgel sample (h-PNIPAM) of $f = 0.092$ and $C = 8$ wt%.

is thus reasonable to consider a power-law model for shear thinning, such as the phenomenological Cross model (Eq. (13)), which displays a plateau, η_0, of the viscosity at low shear rates (corresponding to a linear relationship between stress and shear strain rate at low $\dot{\gamma}$), followed by a power-law shear-thinning regime at intermediate $\dot{\gamma}$, and ultimately a plateau, η_∞, at high $\dot{\gamma}$. The range of the power-law regime, with power-law exponent m, is determined by the time constant τ in Eq. (13).

At low temperatures, we cannot extract a zero-shear viscosity, but at intermediate and high temperatures, we can. However, even at low-temperatures, we can obtain a lower bound on the power law from the *apparent* power law. The best-fit power laws are quite different at different temperatures. At low temperatures, we obtain power laws of $m_{apparent} \approx 0.89$ (see Appendix Fig. A.1). At high temperatures, nearly Newtonian behaviour is observed (i.e., no power-law regime at all). At intermediate temperatures, a power law of $m \approx 0.65$ is obtained from fits to the Cross model (see Appendix Table A.1).

We are most interested in values of the zero-shear viscosity η_0 at all temperatures for which they are obtainable. The corresponding concentrations (and temperatures and crosslink densities) are indicated in green in Appendix Table A.1. Given that the low-shear-rate plateau implies a linear stress-shear rate relationship at low $\dot{\gamma}$, one should obtain consistent values of η_0 from the Cross equation fit to η vs. $\dot{\gamma}$ and from a linear fit to the stress as a function of $\dot{\gamma}$ (at low enough $\dot{\gamma}$). This is indeed the case, as shown in Fig. 4, for observations made on samples prepared at two different concentrations for each of the 4 crosslink densities (the full table of η_0 is shown in Appendix Table A.1, where linear fits alone are denoted with "L" while Cross fits are denoted with a "C"). The fitted power laws for the 4 crosslink densities, remarkably, give values of m that range between 0.6 and 0.69, significantly less than the values of $m_{apparent}$ observed at low temperatures where it is not possible to extract a zero-shear viscosity. We conclude that this intermediate-temperature shear-thinning regime is qualitatively different from the low-temperature gel regime, likely related to the partial collapse of the microgels.

The temperature dependence of the zero-shear viscosity η_0 depends strongly on concentration, C, and crosslink density, f. For example, for a concentration $C = 6$ wt%, the viscosity η_0 reaches a value of 1 Pa.s at 30 °C for $f = 0.011$ (Fig. 4(b)), at less than 25 °C for $f = 0.053$ (Fig. 4(d)), and at 5 °C for $f = 0.092$ (Fig. 4(e)). In order to examine these complex dependences, it is typical to examine the behaviours in terms of a *relative* viscosity $\eta_{rel} = \eta/\eta_s$ (normalizing with respect to the solvent viscosity at the same temperature), and an effective colloid volume fraction Φ_c (to be distinguished from the polymer volume fraction ϕ*inside* the microgel particle). This is the focus of the next section.

4.2. Water and polymer content in soft microgel particles

For each crosslink density, Eq. 12 was applied to calculate $\phi = v_{polymer}/v_{particle}$ from relative viscosity (η_{rel}) measurements for samples in the collapsed state. Then, $v_{particle} = \frac{4}{3}\pi R_H^3$ was used to obtain the factor $v_{polymer}$. Fig. 5(a) shows the average polymer volume in a particle, $\langle v_{polymer} \rangle$, as a function of the particle volume $v_{particle}$ for each of the crosslink densities f in the collapsed state: the relationship is linear with a y-intercept of zero, indicating that in the collapsed state, $\phi = v_{polymer}/v_{particle}$ (Fig. 5(b)) is independent of crosslink density, and has a mean value of 0.40 ± 0.04. This value, interestingly, is consistent with the value $\phi = 0.44$ inferred by Lopez and Richtering [28]. The water volume fraction, $\phi_w = 1 - \phi \sim 0.6$, is higher than a previous estimate for the fraction of "bound water" inside the microgel particle, previously estimated to be about 40% by volume [39]. Since not all the water inside the particle need be "bound" or surface-associated, this is also consistent.

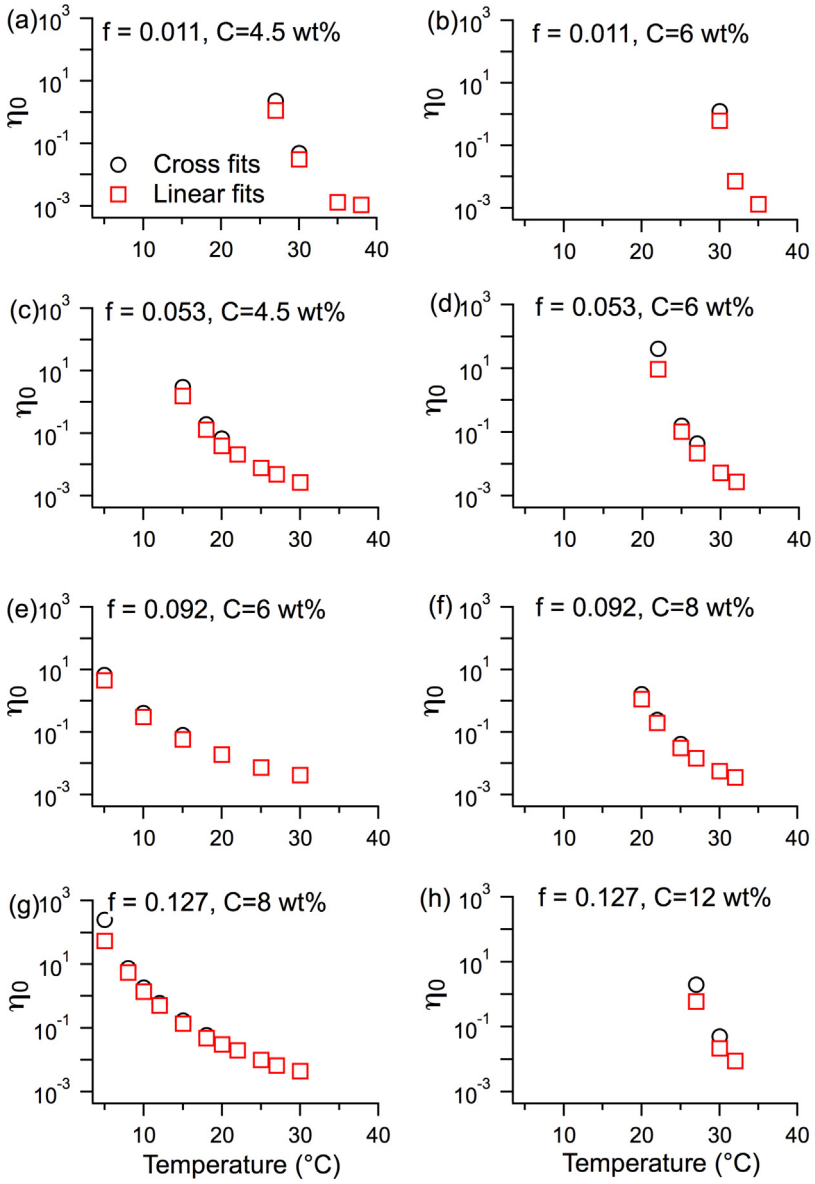

Fig. 4. The zero-shear viscosity, η_0 (in units of Pa.s) obtained by both Cross and linear fits, *versus* temperature for the eight samples of microgels at cross-linker densities f and sample concentrations C given by (a) f = 0.011, C = 4.5 wt% (b) f = 0.011, 6 wt% (c) f = 0.053, C = 4.5 wt% (d) f = 0.053, 6 wt% (e) f = 0.092, C = 6 wt% (f) f = 0.092, 8 wt% (g) f = 0.127, C = 8 wt% (h) f = 0.127, C = 12 wt%. The results from Cross fits and linear fits are plotted in black circles, and red squares, respectively. Error bars, calculated from standard deviations from the mean value, are plotted but not visible because they are smaller than the symbols. (For interpretation of the references to colour in this figure legend, the reader is referred to the web version of this article.)

Using the polymer volume fraction at 45 °C (Fig. 5)) and the temperature dependence of the microgel particle size R_H (Fig. 1), we can estimate both the polymer volume fraction ϕ and the water volume fraction $\phi_w = 1 - \phi$ as a function of temperature. Note that the total polymer volume per particle, v_{polymer}, is temperature independent; all of the temperature dependence comes from the temperature dependence of v_{particle}, which in the dilute limit can be assumed to be spherical, $v_{\text{particle}}(T) = \frac{4}{3}\pi R_H(T)^3$. We see (Fig. 5(c)) that the fraction of water is large: $\phi_w \equiv 1 - \phi \approx 0.6$ in the collapsed state ($T = 45$ °C), while $\phi \approx 0.4$, The values of ϕ decrease dramatically, and those of ϕ_w concomitantly increase, as temperature is lowered through the transition. At $T = 5$ °C, ϕ ranges from 0.02 to 0.09 with increasing f, while ϕ_w ranges from 0.98 to 0.91 with increasing f.

Given $\langle v_{\text{polymer}} \rangle$ as a function of crosslink density, one can also self-consistently, using Eq. 10, obtain an "effective" packing fraction $\Phi_{c,\text{eff}}$ for all sample concentrations and crosslink densities. This is, of course, a fictitious packing fraction anywhere outside of the dilute system/collapsed state region, but is a useful quantity to assess deviations from the hard-sphere paradigm. The *relative* viscosity $\eta_{\text{rel}} = \eta/\eta_s$ is plotted as a function of $\Phi_{c,\text{eff}}$ in Fig. 6 for all microgel samples at all crosslink densities, f = 0.011, 0.053, 0.092 and 0.127 (i.e., m_{BIS}/m_{NIPAM} = 1.5, 7.5, 13.6, and 19.5 wt%). It is seen in Fig. 6 that all datasets are in agreement with hard-sphere behaviour (as exemplified by the Krieger-Dougherty relation, or "KD line"), not just for the samples at the highest temperature, but for all samples and conditions corresponding to $\Phi_{c,\text{eff}} < 0.4$. Beyond this packing fraction, it is observed that the lowest crosslink density $f = 0.011$ deviates the most from hard-sphere behaviour while the highest crosslink densities f = 0.092 and 0.127 are the closest to the KD line.

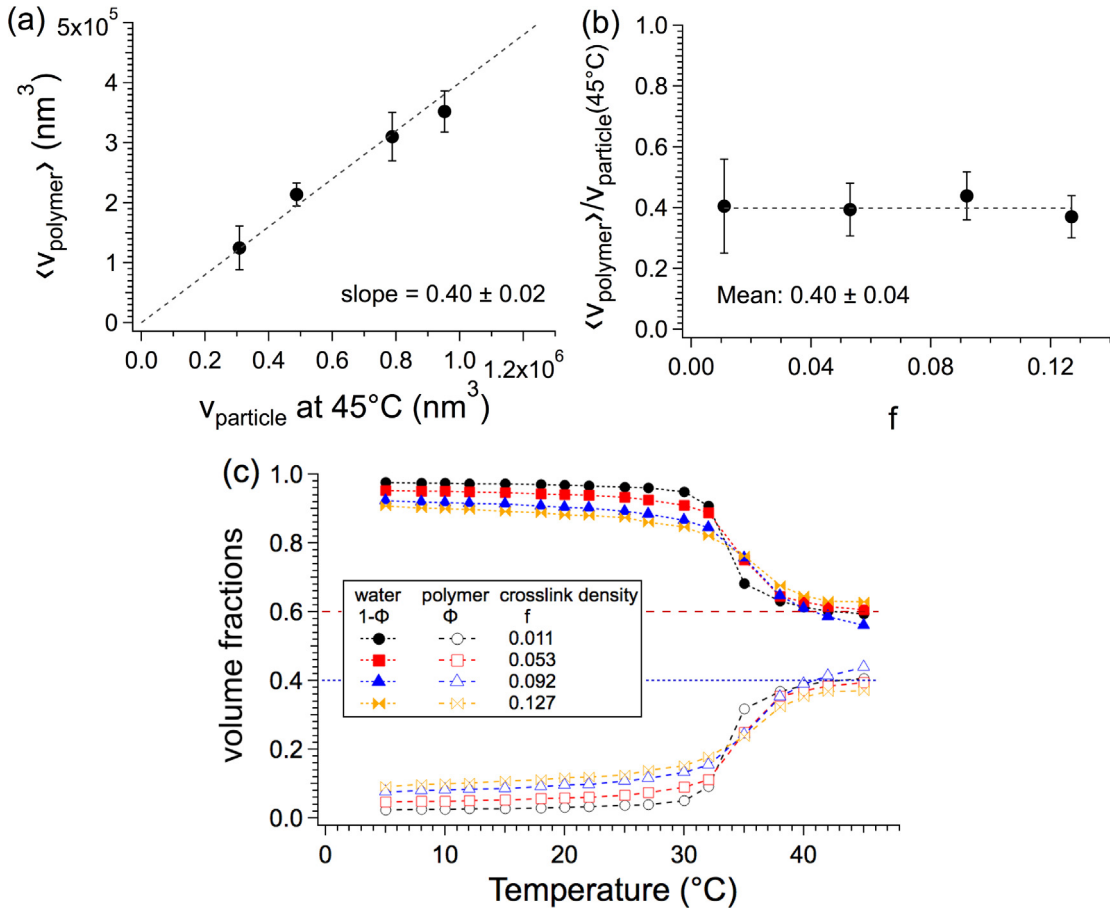

Fig. 5. (a) Average calculated polymer volume in a microgel particle, $\langle v_{polymer} \rangle$, for different f *versus* the particle volume at 45 °C at the 4 crosslink densities: the highest $v_{particle}$ corresponds to the lowest f. For a given f, the polymer volume $v_{polymer}$ is temperature independent. (b) The $(v_{polymer}/v_{particle}(45\,^{\circ}C))$ ratio is independent of f. (c) The polymer volume fraction in the particle $\phi \equiv v_{polymer}/v_{particle}$ and the water volume fraction $1-\phi$, plotted as a function of temperature for 4 crosslink densities, using the result in (b) and the collapse curves in Fig. 1.

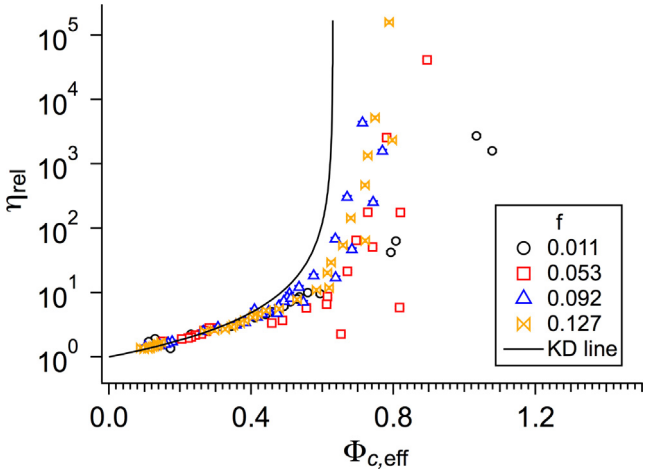

Fig. 6. Dependence of the relative viscosity on the effective volume fraction $\Phi_{c,eff}$, for all the microgels samples at different C, T and f. The Krieger-Dougherty (KD) line was plotted for comparison to the colloidal suspension hard sphere behavior.

4.3. Gel-swelling and DLS

We are now ready to examine our dynamic light scattering results at low concentrations in the context of gel-swelling phenomenology, as promised earlier. We fit the DLS results for the hydrodynamic radius R_H for both h- and d3-PNIPAM and all 4 crosslink densities. In order to carry out this fit robustly, we use Eq. 5, which has numerous fit parameters, A, C, D, θ, ϕ_0, along with the parameters in Eq. 1 to convert ϕ to the observed R_H, i.e., $\phi_{collapse}$ and $R_{collapse}$. We adopt the following criteria:

1. the polymer concentration in the collapsed state is held at $\phi_{collapse} = 0.4$.
2. the θ temperature is held (following Lopez et al. [28]) at the linear polymer chain value, 303.8 K for h-NIPAM [40] and based on our results (Table 1), approximately 1.2 K higher for d3-NIPAM, thus 305 K.
3. ϕ_0 is not constrained to be $\phi_{collapse}$.
4. the molar fraction of crosslinker f is set to its known value for each crosslink density (see Table 1).
5. The term containing the parameter D, which is the highest order term, is omitted from the reported fit based on an observation that the quality of fits carried out with D included were insensitive to its value.
6. 8 datasets – 4 crosslink densities, h- and d3-PNIPAM, each with an identical number (17) of sampling temperatures – are fit using a global fitting routine.

The collapse curves, and the Flory-Rehner fits, are shown in Fig. 7. The fits are reasonably good, but more importantly with so many fit parameters, they are robust. There is a noticeable overshoot in the Flory-Rehner fit at the lowest crosslink density (which has the largest change in swelling factors at the collapse transition,

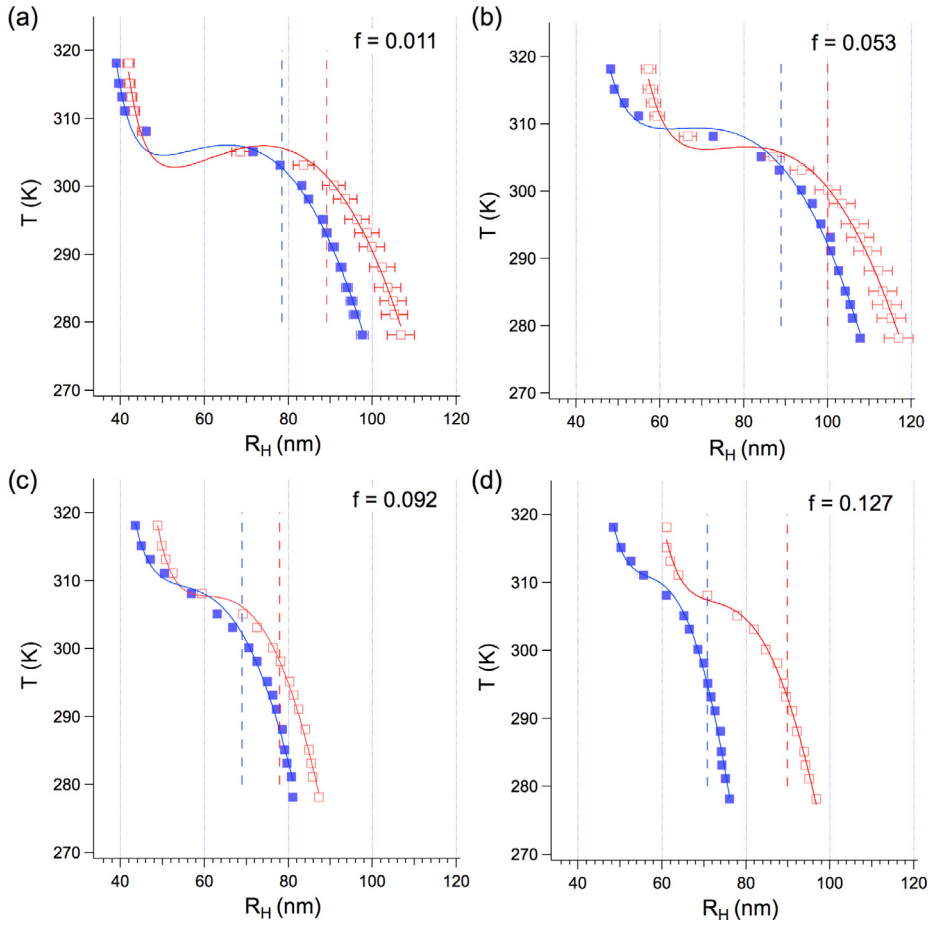

Fig. 7. Fit of the DLS collapse curves, plotted as T (in K) vs. R_H to Flory-Rehner theory for crosslinks densities f = (a) 0.01 (b) 0.053 (c) 0.092 (d) 0.127. The h-PNIPAM nad d3-PNIPAM are shown in open red and solid blue square symbols respectively, while the fits are the solid red and blue lines. The vertical dashed lines indicate the particle hydrodynamic radius $R_{H,cross}$ when $\phi/\phi_0 = 2^{3/2}$, and the elastic term in Eq. (4) is zero. (For interpretation of the references to colour in this figure legend, the reader is referred to the web version of this article.)

and this overshoot is significantly diminished at higher crosslink densities. The overshoot represents the possibility of multiple hydrodynamic radii for a single temperature, and is not seen experimentally. The hydrodynamic radius is, of course, directly inversely related to ϕ and thus the particle density, which is a relevant order parameter for the collapse transition.

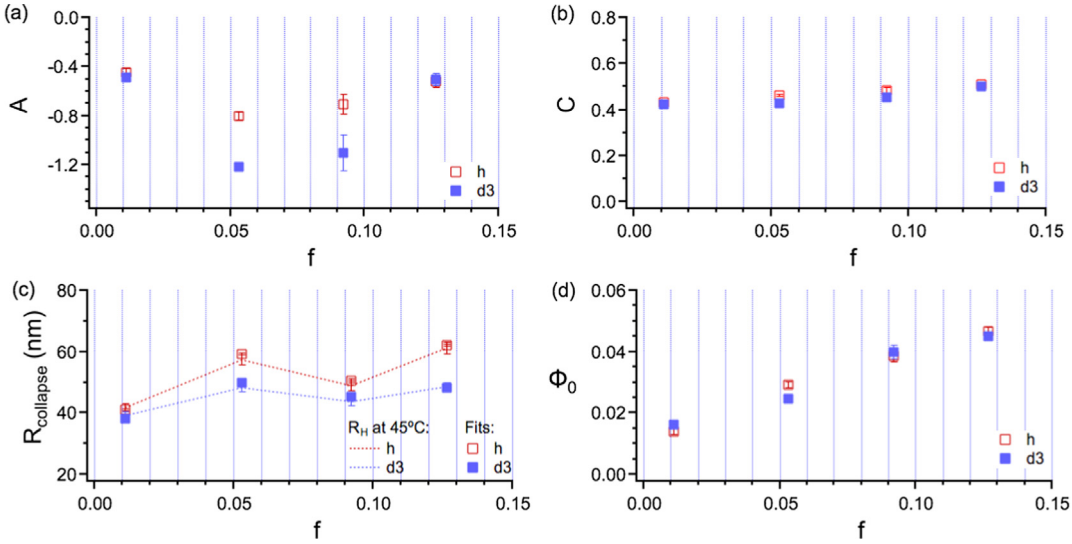

Fig. 8. The parameters of the fit to Flory-Rehner theory as a function of crosslink density f. The h-PNIPAM and d3-PNIPAM are shown in open red and solid blue square symbols respectively. (a) The A parameter.which is a prefactor of the second virial coefficient is negative, of order unity, and roughly independent of f. (b) The phenomenological expansion parameters for χ. (c) The fitted value of the hydrodynamic radius at collapse, $R_{collapse}$, increases with f. Also shown (dotted lines) are the raw values for R_H obtained at $T = 45$ °C. (d) The reference polymer volume fraction ϕ_0 shows a systematic increase, from 0.02 to 0.06, with increasing f, for both h- and d3-PNIPAM samples. (For interpretation of the references to colour in this figure legend, the reader is referred to the web version of this article.)

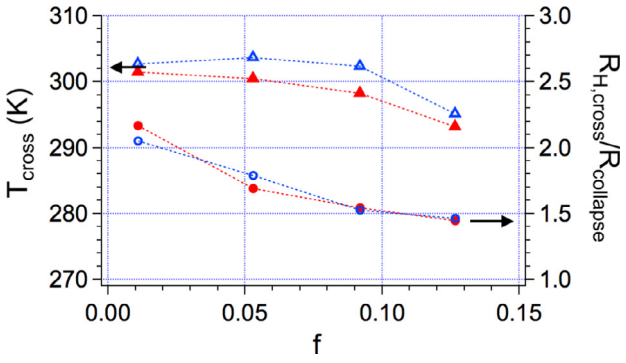

Fig. 9. The crossover temperature (left) and hydrodynamic radius for each microgel system where the elastic term in Eq. (4) (based on the fitted Flory-Rehner parameters) changes sign. Red/blue symbols: h/d3-NIPAM. (For interpretation of the references to colour in this figure legend, the reader is referred to the web version of this article.)

Next, we examine in Fig. 8 the dependence of the fit parameters on the crosslink density, for both h-PNIPAM and d3-PNIPAM samples. The parameter A (Fig. 8(a)) varies between −0.4 and −1.1, and is most negative, i.e. has a larger magnitude of interparticle interactions, at intermediate f. The parameter C changes only a little across all datasets: C varies between 0.4 and 0.5 with a small increase with crosslink density. The fitted value of the hydrodynamic radius at collapse (Fig. 8(c), symbols) shows an increase with f, and is somewhat higher than the raw value for R_H (Fig. 8 (c), dotted lines) obtained at the highest temperature ($T = 45\,^{\circ}C$) for each sample. The increase in $R_{collapse}$ is not monotonic. It is possible that the absolute particle size is sensitive to small but uncontrolled variations in the synthesis conditions. The ϕ_0 parameter exhibits a steady increase with f, rising from 0.02 to 0.06, with not too much difference between the h-PNIPAM and d3-PNIPAM samples. This implies that the ratio $\phi_{collapse}/\phi_0$ ranges from 20 (for the lowest f) to 6.7 (for the highest f). This number is directly comparable to the swelling factors plotted in Fig. 2, and suggests that ϕ_0 is more representative of the polymer volume fraction at low temperatures.

This point is worth examining in a bit more detail. The result that $\phi_0 \ll \phi_{collapse}$ implies that there are many temperatures where $\phi > \phi_0$, and the elastic contribution to the osmotic pressure (shown in Eq. 4) can be positive as well as negative. There is a particular value (R_H, T), corresponding to $\phi/\phi_0 = 2^{3/2}$, where this term is zero. At higher temperatures (smaller R_H), this term is positive, while at lower temperatures (larger R_H) this term is negative. Fig. 9 shows the crossover temperature T_{cross} (left axis) and the corresponding particle size at crossover relative to the collapsed state, $R_{H,cross}/R_{collapse}$ (right axis), as a function of crosslink molar fraction f. The crossover temperature, where the elasticity term is zero, decreases a little (but systematically) with increasing crosslink density. Moreover, the T_{cross} curve for d3-NIPAM is shifted up by roughly 1–3 K from that for h-NIPAM which is the difference in the θ temperature for the two polymers. $R_{H,cross}/R_{collapse}$, on the other hand, decreases from a value of 2 to a value of 1.4 with increasing crosslink density for both h-NIPAM and d3-NIPAM.

5. Conclusions

In this work, we have first used rheology to obtain the real polymer volume fraction ϕ, in the collapsed state, of microgel particles at four different crosslink densities. We find this polymer volume fraction to be $\phi_{collapse} = 0.40 \pm 0.04$, independent of crosslink density. We couple this with dynamic light scattering determinations of particle hydrodynamic radius R_H as a function of temperature T, and obtain the polymer and water volume fractions as a function of temperature.

While the above assumes uniform, spherical microgels, the microgel density is in principle not uniform; e.g., recent super-resolution microscopy [24] clearly shows a core-shell morphology. Our rheological determination of ϕ is still reasonable however because the analysis is based on high temperatures for which the particle is in the collapsed state and the particle density is more uniform. We find consistency between particle molecular weights calculated using our knowledge of the collapsed particle size and those determined from static light scattering (see Appendix A.4 and Fig. A.3).

Using the polymer volume fraction, we then calculate an effective particle packing fraction $\Phi_{c,eff}$, a collective suspension property distinct from the polymer volume fraction ϕ, which is a single-particle property. The implicit assumption is that the particles are hard-sphere-like. We find, self-consistently, that the relative viscosity $\eta_{rel} = \eta_0/\eta_s$ for all crosslink densities collapses onto a single curve that is in agreement with hard-sphere behavior (the Krieger-Dougherty line) provided the suspensions are dilute enough, i.e., for $\Phi_{c,eff} < 0.4$. Above $\Phi_{c,eff} = 0.4$, all microgels (see Appendix A.4 and Fig. A.3) deviate from hard-sphere behavior, with the microgels at the lowest crosslink density deviating most.

Again using the polymer volume fraction at collapse, we are able to obtain robust fits of T *versus* R_H in the context of the Flory-Rehner theory for gel swelling. The key advantage in our approach is that we are able to constrain $\phi_{collapse}$, and globally fit 8 datasets corresponding to 4 crosslink densities for protonated h-PNIPAM and deuterated d3-PNIPAM microgels. It is interesting to examine the sensitivity of the fit parameters to crosslink density and deuteration. $R_{collapse}$ is distinct from the other parameters in that it is the particle size at collapse, while the others relate to particle properties. The parameter C, which is a phenomenological term, shows only a very weak increase with crosslink density f (and is identical for protonated and deuterated PNIPAM). The other terms, which are physically meaningful, all show dependences. The reference polymer volume fraction ϕ_0 shows a clear increase with f, and is very similar for protonated and deuterated variants. The remaining two parameters are sensitive to both f and deuteration. The A term, which is related to the second virial coefficient, is most negative at intermediate f, while the microgel size $R_{collapse}$ shows an increasing trend with f.

The Flory–Rehner hypothesis (see chapter XI in Flory's classic text [30]) is that the thermodynamics of polymeric gels can be split up into two independent contributions, the mixing contribution and the elastic contribution; this assumption is also common to other more recent approaches (see [26]). Moreover, each gel has a unique reference volume fraction ϕ_0, which corresponds to the volume occupied by the polymer when crosslinks were introduced into the system. Given the conditions of synthesis (see Section 3.1) most of the crosslinking proceeds at 70 °C, i.e., in the collapsed state. It should be noted, however, that crosslinking could continue to occur while cooling slowly to room temperature (20 °C).

It is thus not consistent with the above hypothesis that one obtains a ϕ_0 that varies from 0.02 to 0.06 with increasing crosslink density. These low values of reference volume fraction correspond with temperatures less than 10 °C; for example, ϕ at $T = 5\,^{\circ}C$ (i.e., in the swollen state) is numerically comparable to the fitted value of ϕ_0 shown in Fig. 8(d). It has been pointed out [26] that several groups have inferred different reference states: some find low-temperature reference states [41,42,28] (with $\phi_0 \sim 0.03$–0.07) while many obtain much higher ϕ_0 (see Table A.1 in [28] for a list). The latter (i.e., higher ϕ_0) is consistent with the original hypothesis of Flory and Rehner that ϕ_0 corresponds to the volume occupied by the polymer when crosslinks were introduced.

We thus look at the behavior of the elastic term of the Flory-Rehner theory (Eq. 4) which is crucial for fitting the collapse curves. We find, interestingly, that it changes sign at a crossover temperature between 293 K and 306 K (depending on crosslink density and deuteration). This range of crossover temperatures is close both to the final temperature of the synthesis and to the θ temperature. In particular, there is a systematic shift between crossover temperatures of protonated and deuterated PNIPAM that is very close to the difference in θ temperature. We do not understand these dependences at this time, but hope that it will provoke more thought.

In future, any theory that quantitatively captures the collapse curves should capture these systematic dependences on solvent quality. In addition, one could learn more, experimentally, about ϕ_0 by tracking R_H during the synthesis (as done by Gao et al. [43]). Ongoing work in our group focuses on the study of internal polymer dynamics in d3- and d7-PNIPAM microgel colloids as a function of temperature and pressure, using deuterium NMR.

Appendix A. Results of the fit to the cross equation

A.1. The power law, m_{apparent}

The *apparent slope* $m_{\text{apparent}} \equiv -\frac{d(\log\eta)}{d(\log\dot\gamma)}$ at a given shear rate, is related to the Cross exponent m by.

$$m_{\text{apparent}} = -\frac{d(\log\eta)}{d(\log\dot\gamma)} = \left[\frac{(\eta_0-\eta_\infty)(\dot\gamma\tau)^m}{\left(\eta_\infty+\frac{\eta_0-\eta_\infty}{1+(\dot\gamma\tau)^m}\right)\left(1+(\dot\gamma\tau)^m\right)^2}\right]m. \qquad (A.1)$$

When $\eta_0 \gg \eta_\infty(\dot\gamma\tau)^m$ and $\dot\gamma\tau \gg 1$, the term in square brackets is unity, and otherwise it is less than 1. It can be seen that for a given temperature, m_{apparent} depends on the range of the shear rate over which it is calculated.

In Fig. A.1(a), the slope m_{apparent} is plotted for windows of increasing $\dot\gamma$, while Fig. A.1(b) plots the maximum value of m_{apparent} for each curve. It is seen that at $m_{\text{apparent}} \approx 0.89$ for $T \leqslant 15\,^\circ$C but decreases with increasing temperature. We have no *a priori* reason, apart from simplicity, to expect the power law m to be independent of temperature, because the particle softness is expected to be temperature dependent. For all data that exhibit distinct low and high temperature plateaus in η, we can fit to the Cross model. For reasons of simplicity we constrain m for a given sample (i.e., for a given f and C) to a single value for all temperatures in this regime, and fit for η_0, η_∞ and τ.

A.2. Table of fit parameters

For completeness, a list of all the fitted zero-shear viscosities, η_0, are tablulated in Table A.1 for all the temperatures where there was a plateau in viscosity when approaching zero shear rate. Temperature and sample concentration conditions where Cross fits were possible, i.e., where samples exhibited a zero-shear plateau, followed by shear-thinning and a high-shear plateau, are highlighted in green in the table and indicated by "C" in the type of fit. In regimes where Newtonian behaviour was observed (indicated by "L" in the fit column), a simple linear fit of stress *versus* strain rate was carried out to obtain η_0.

A.3. Flory-Rehner fits

In this work, we found that the fitted value for the reference volume fraction ϕ_0 was much lower ϕ_{collapse}. We examine this point by setting $\phi_0 = \phi_{\text{collapse}}$. The resulting fit (Fig. A.2) is poor, and the fitted values of ϕ_{collapse} and R_{collapse} are unphysical.

A.4. Particle molecular weights

The microgel particles are assumed, for the purposes of this study, to be uniform in density profile. We check consistency of this result by comparing molecular weights calculated from the hydrodynamic radius at collapse for h-PNIPAM microgels with that obtained from static light scattering. For the calculated molecular weight we use

$$M_w = 10^3 \times \rho_{\text{PNIPAM}} N_A (4\pi/3) R^3_{\text{collapse}} \phi_{\text{collapse}} \qquad (A.2)$$

(in units of g/mole), where N_A is the Avogadro number and $\rho = 1.1\times10^3$ kg/m^3 is the density of PNIPAM polymer. ϕ_{collapse} is set to 0.4.

The molecular weight is also obtained from static light scattering experiments for h-PNIPAM microgels, Static light scattering (SLS) studies (Photocor Ltd., Russia) were carried out at a wavelength of 633 nm. Experimental are carried out at a very low sample concentrations in order to avoid particle interactions. In our SLS studies, the scattering intensity of the microgel suspension prepared at low concentration is measured as a function of scattering angle (theta) between 15 and 130° in the swollen state at 20 °C. The excess of scattering intensity is measured with respect to solvent (deionized water). The absolute scattering intensity, the excess Rayleigh ratio (cm^{-1}) is deduced using a toluene as a refer-

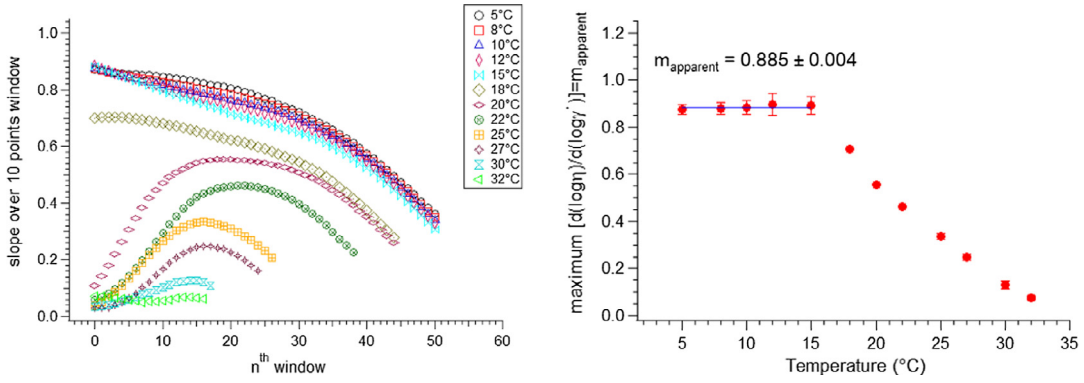

Fig. A.1. (a) The slope test results with the 10 points window width, for all temperatures. This is done for the microgel sample of $f = 0.092$ and $C = 8$ wt% steady flow data. (b) The *apparent* power law exponent (from the slope test results) for the microgel sample of $f = 0.092$ and $C = 8$ wt%, as a function of temperature: m_{apparent} is constant (with a value $m_{\text{apparent}} \approx 0.89$) for $T \leqslant 15\,^\circ$C, and decreases at higher temperatures.

Table A.1
The obtained η_0 values, along with the type of fit that was used to determine them ("L" for linear fit, and "C" for Cross fit) for all the 16 samples at different f, C, and T (°C). The η_s values as a function of temperature are listed as well, in the first Section to the left. For the samples were Cross fits had been used, highlighted in green, the m values as obtained by the Cross fits are listed.

Water		f = 0.001				f = 0.053				f = 0.092				f = 0.127			
T (°C)	η_S (mPa.s)	C (wt%)	T (°C)	η_0 (mPa.s)	fit	C (wt%)	T (°C)	η_0 (mPa.s)	fit	C (wt%)	T (°C)	η_0 (mPa.s)	fit	C (wt%)	T (°C)	η_0 (mPa.s)	fit
5	1.55 (8)	1.5	5	16 (1)	L	1.5	5	4.4 (2)	L	1.5	5	2.7 (1)	L	1.5	5	2.6 (1)	L
8	1.43 (7)		8	12 (1)	L		8	4.0 (2)	L		10	2.1 (1)	L		8	2.3 (1)	L
10	1.36 (7)		10	11 (1)	L		10	3.4 (2)	L		15	1.9 (1)	L		10	2.1 (1)	L
12	1.28 (6)		12	9.2 (5)	L		12	3.3 (2)	L		20	1.5 (1)	L		12	1.9 (1)	L
15	1.18 (6)		15	7.2 (4)	L		15	2.7 (1)	L		25	1.3 (1)	L		15	1.7 (1)	L
18	1.09 (5)		18	5.5 (3)	L		18	2.4 (1)	L		30	1.1 (1)	L		18	1.6 (1)	L
20	1.03 (5)		20	4.7 (2)	L		20	2.1 (1)	L	4.5	5	19 (1)	L		20	1.4 (1)	L
22	0.97 (5)		22	4.0 (2)	L		22	1.9 (1)	L		8	14 (1)	L		22	1.3 (1)	L
25	0.90 (4)		25	3.1 (2)	L		25	1.7 (1)	L		10	11 (1)	L		25	1.2 (1)	L
27	0.85 (4)		27	2.5 (1)	L		30	1.4 (1)	L		12	9.4 (5)	L		27	1.1 (1)	L
30	0.78 (4)		30	2.1 (1)	L	4.5	15	30 (2) E2	C 0.64 (1)		15	7.2 (4)	L		30	1.1 (1)	L
32	0.74 (4)	4.5	27	23 (1) E2	C 0.62 (1)		18	19 (1) E1	C		18	5.6 (3)	L	4.5	5	8.1 (4)	L
35	0.68 (3)		30	49 (2)	C		20	66 (3)	C		20	4.8 (2)	L		8	6.6 (3)	L
38	0.63 (3)		35	1.3 (1)	L		22	21 (1)	L		22	4.1 (2)	L		10	6.0 (3)	L
			38	1.1 (1)	L		25	7.8 (4)	L		25	3.1 (2)	L		12	5.3 (3)	L
		6	30	12 (1) E2	C/0.60(1)		27	4.9 (2)	L		27	2.7 (1)	L		15	4.4 (2)	L
			32	7.1 (4)	L		30	2.6 (1)	L		30	2.2 (1)	L		18	3.6 (2)	L
			35	1.3 (1)	L	6	22	40 (2) E3	C 0.66 (0)		32	1.8 (1)	L		20	3.2 (2)	L
		8	32	31 (2)	L		25	16 (1) E1	C	6	5	67 (3) E2	C 0.67 (1)		22	2.9 (1)	L
			35	1.5 (1)	L		27	43 (2)	C		10	41 (2) E1	C		25	2.4 (1)	L
							30	5.2 (3)	L		15	80 (4)	C		27	2.2 (1)	L
							32	2.7 (1)	L		20	19 (1)	L		30	2.0 (1)	L
						8	30	4.6 (2)	L		25	7.3 (4)	L	8	5	25 (1) E4	C
							32	1.7 (1)	L		30	4.3 (2)	L		8	75 (4) E2	C
										8	20	16 (1) E2	C 0.68 (1)		10	18 (1) E2	C 0.69 (0)
											22	25 (1) E1	C		12	60 (3) E1	C
											25	42 (2)	C		15	17 (1) E1	C
											27	15 (1)	L		18	59 (3)	C
											30	5.6 (3)	L		20	30 (2)	L
											32	3.5 (2)	L		22	20 (1)	L
															25	9.9 (5)	L
															27	6.6 (3)	L
															30	4.4 (2)	L
														12	27	20 (1) E2	C 0.65 (1)
															30	50 (2)	C
															32	8.8 (4)	L

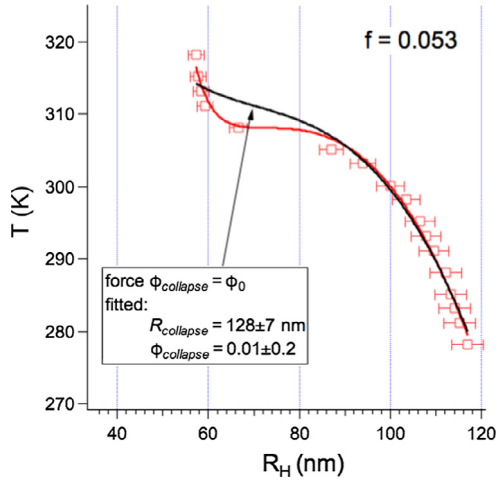

Fig. A.2. Carrying out a fit with $\phi_0 = \phi_{\text{collapse}}$ yields a poor fit, and unphysical values of both ϕ_{collapse} and R_{collapse}.

ence sample whose Rayleigh ratio is, $R_{toluene} = 1.35 \times 10^{-5}$ cm^{-1} at 633 nm. The excess Rayleigh ratio $R(\theta)$ of microgel suspension at different concentrations can be calculated using

$$R(\theta) = (I_{sus}(\theta) - I_{sol}(\theta))/I_{tol}(\theta)[(n_{solvent}/n_{toluene})^2]R_{toluene}. \quad (A.3)$$

I_{sus}, I_{sol} and I_{tol} are the scattering intensity of suspension, solvent, and toluene reference. $n_{solvent} = 1.3314$ and $n_{toluene} = 1.49$ are the refractive index of the solvent and toluene, respectively, at 20 °C. Under weak particle interactions, the weight-average molecular weight, M_w is related to excess Rayleigh ratio, $R(\theta)$ is given by the expression [44]

$$KC/R(\theta) = 1/M_w + (R_g^2/3M_w)(16\pi^2 n_{solvent}^2/\lambda^2)\sin^2(\theta/2), \quad (A.4)$$

where $K = 4\pi n_{solvent}^2 (dn/dc)^2/(\lambda^4 N_A)$ is an optical constant, C is the microgel concentration in g/ml, dn/dC = 0.167 ml/gm is the refractive index increment of microgels in the swollen state [45] and N_A is the Avogadro number.

The comparison of molecular weights from the two methods is shown in Fig. A.3. The agreement suggests that assuming uniform spheres is reasonable.

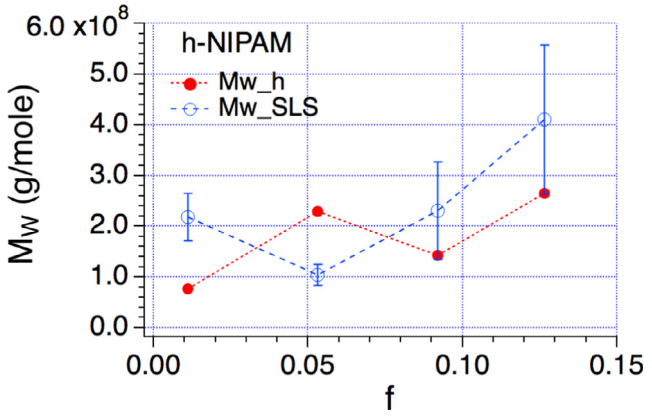

Fig. A.3. Comparison of molecular weights obtained from calculation (based on assuming a uniform sphere) and from static light scattering measurements, for h-PNIPAM microgels at all crosslink densities.

References

[1] P. Pusey, W. Van-Megen, Phase behavior of concentrated suspensions of nearly hard colloidal spheres, Nature 320 (1986) 340–342.
[2] Y. Monovoukas, A.P. Gast, The experimental phase diagram of charged colloidal suspensions, J. Colloid Interface Sci. 128 (1989) 533–548.
[3] A. van Blaaderen, P. Wiltzius, Real-space structure of colloidal hard-sphere glasses, Science 270 (1995) 1177–1179.
[4] A.P. Gast, W.B. Russel, Simple ordering in complex fluids, Phys. Today 51 (1998) 24–31.
[5] U. Gasser, E.R. Weeks, A. Schofield, P. Pusey, D. Weitz, Real-space imaging of nucleation and growth in colloidal crystallization, Science 292 (2001) 258–262.
[6] A. Yethiraj, A. van Blaaderen, A colloidal model system with an interaction tunable from hard sphere to soft and dipolar, Nature 421 (2003) 513–517.
[7] A.M. Alsayed, M.F. Islam, J. Zhang, P.J. Collings, A.G. Yodh, Premelting at defects within bulk colloidal crystals, Science 309 (2005) 1207–1210.
[8] A. Yethiraj, Tunable colloids: control of colloidal phase transitions with tunable interactions, Soft Matter 3 (2007) 1099–1115.
[9] P.S. Mohanty, P. Bagheri, S. Nojd, A. Yethiraj, Multiple path-dependent routes for phase-transition kinetics in thermoresponsive and field-responsive ultrasoft colloids, Phys. Rev. X (2015) 53–55.
[10] M. Murray, M. Snowden, The preparation, characterisation and applications of colloidal microgels, Adv. Colloid Interface Sci. 54 (1995) 73–91.
[11] L.A. Lyon, A. Fernández-Nieves, The polymer/colloid duality of microgel suspensions, Annu. Rev. Phys. Chem. 63 (2012) 25–43.
[12] H. Senff, W. Richtering, Temperature sensitive microgel suspensions: colloidal phase behavior and rheology of soft spheres, J. Chem. Phys. 111 (1999) 1705–1711.
[13] H. Senff, W. Richtering, Influence of cross-link density on rheological properties of temperature-sensitive microgel suspensions, Colloid Polym. Sci. 278 (2000) 830–840.
[14] P.S. Mohanty, W. Richtering, Structural ordering and phase behavior of charged microgels, J. Phys. Chem. B 112 (47) (2008) 14692–14697.
[15] P.J. Yunker, K. Chen, M.D. Gratale, M.A. Lohr, T. Still, A.G. Yodh, Physics in ordered and disordered colloidal matter composed of poly(N-isopropylacrylamide) microgel particles, Rep. Prog. Phys. 77 (2014) 056601.
[16] J. Lietor-Santos, B. Sierra-Martin, U. Gasser, A. Fernandez-Nieves, The effect of hydrostatic pressure over the swelling of microgel particles, Soft Matter 7 (2011) 6370–6374.
[17] P. Mohanty, A. Yethiraj, P. Schurtenberger, Deformable particles with anisotropic interactions: unusual field-induced structural transitions in ultrasoft ionic microgel colloids, Soft Matter 8 (2012) 10819–10822.
[18] D. Vlassopoulos, M. Cloitre, Tunable rheology of dense soft deformable colloids, Curr. Opin. Colloid Interface Sci. 19 (2014) 561–574.
[19] D. Gottwald, C. Likos, G. Kahl, H. Löwen, Phase behavior of ionic microgels, Phys. Rev. Lett. 92 (2004) 068301.
[20] I. Varga, T. Gilányi, R. Meszaros, G. Filipcsei, M. Zrinyi, Effect of cross-link density on the internal structure of poly (n-isopropylacrylamide) microgels, J. Phys. Chem. B 105 (2001) 9071–9076.
[21] T. Hellweg, K. Kratz, S. Pouget, W. Eimer, Internal dynamics in colloidal PNIPAM microgel particles immobilised in mesoscopic crystals, Colloids Surfaces A: Physicochem. Eng. Asp. 202 (2002) 223–232.
[22] B. Sierra-Martín, Y. Choi, M.S. Romero-Cano, T. Cosgrove, B. Vincent, A. Fernández-Barbero, Microscopic signature of a microgel volume phase transition, Macromolecules 38 (2005) 10782–10787.
[23] J. Retama, B. Frick, T. Seydel, M. Stamm, A. Barbero, E. Cabarcos, Polymer chain dynamics of core-shell thermosensitive microgels, Macromolecules 41 (2008) 4739–4745.
[24] G. Conley, S. Nöjd, M. Braibanti, P. Schurtenberger, F. Scheffold, Superresolution microscopy of the volume phase transition of pNIPAM microgels, Colloids Surfaces A: Physicochem. Eng. Asp. 499 (2016) 18–23. Available from: arXiv:1512.00414.
[25] M. Karg, S. Prévost, A. Brandt, D. Wallacher, R. von Klitzing, T. Hellweg, Poly-nipam microgels with different cross-linker densities, in: Intelligent Hydrogels, Springer, 2013, pp. 63–76.
[26] M. Quesada-Pérez, J.A. Maroto-Centeno, J. Forcada, R. Hidalgo-Alvarez, Gel swelling theories: the classical formalism and recent approaches, Soft Matter 7 (2011) 10536–10547.
[27] M. Urich, A.R. Denton, Swelling, structure, and phase stability of compressible microgels, Soft Matter 12 (2016) 9086–9094.
[28] C.G. Lopez, W. Richtering, Does Flory-Rehner theory quantitatively describe the swelling of thermoresponsive microgels, Soft Matter 13 (2017) 8271–8280.
[29] V. Nigro, R. Angelini, M. Bertoldo, B. Ruzicka, Swelling of responsive-microgels: experiments versus models, Colloids Surfaces A: Physicochem. Eng. Asp. 532 (2017) 389–396.
[30] P. Flory, Principles of Polymer Chemistry, Cornell University Press, Ithaca, 1953.
[31] M. Rubinstein, R.H. Colby, Polymer Physics, Oxford University Press, New York, 2003.
[32] J. Liétor-Santos, B. Sierra-Martín, R. Vavrin, Z. Hu, U. Gasser, A. Fernández-Nieves, Deswelling microgel particles using hydrostatic pressure, Macromolecules 42 (2009) 6225–6230.
[33] Note that the factor Φ_c/C ≈k is used in the literature to convert from mass concentration to packing fraction. This approximate relation is consistent with Equation 10 provided that C is much less than 1, which is indeed usually the case.
[34] I. Krieger, T. Dougherty, A mechanism for non-Newtonian flow in suspensions of rigid spheres, Trans. Soc. Rheol. 3 (1959) 137–152.
[35] J. Bicerano, J.F. Douglas, D.A. Brune, Model for the viscosity of particle dispersions, Rev. Macromol. Chem. Phys. C 39 (1999) 561–642.
[36] M. Cross, Rheology of non-Newtonian fluids: a new flow equation for pseudoplastic systems, J. Colloid Interface Sci. 20 (1965) 417–437.
[37] U. Gasser, J. Hyatt, J. Lietor-Santos, E. Herman, L. Lyon, A. Fernandez-Nieves, Form factor of pNIPAM microgels in overpacked states, J. Chem. Phys. 141 (2014) 034901.
[38] D. Sessoms, I. Bischofberger, L. Cipelletti, V. Trappe, Multiple dynamic regimes in concentrated microgel systems, Philos. Trans. R. Soc. A 367 (2009) 5013–5032.
[39] A. Lele, M. Hirve, M. Badiger, R. Mashelkar, Predictions of bound water content in poly (n-isopropylacrylamide) gel, Macromolecules 30 (1997) 157–159.
[40] K. Kubota, S. Fujishige, I. Ando, Solution properties of poly (n-isopropylacrylamide) in water, Polym. J. 22 (1990) 15–20.
[41] S. Hirotsu, Y. Hirokawa, T. Tanaka, Volume-phase transitions of ionized n-isopropylacrylamide gels, J. Chem. Phys. 87 (2) (1987) 1392–1395.
[42] L. Bromberg, M. Temchenko, G.D. Moeser, T.A. Hatton, Thermodynamics of temperature-sensitive polyether-modified poly (acrylic acid) microgels, Langmuir 20 (14) (2004) 5683–5692.
[43] J. Gao, B.J. Frisken, Cross-linker-free n-isopropylacrylamide gel nanospheres, Langmuir 19 (2003) 5212–5216.
[44] M.B. Huglin (Ed.), Light Scattering from Polymer Solutions, Academic Press, New York, 1972.
[45] L. Arleth, X. Xia, R.P. Hjelm, J. Wu, Z. Hu, Volume transition and internal structures of small poly (n-isopropylacrylamide) microgels, J. Polym. Sci. Part B: Polym. Phys. 43 (7) (2005) 849–860.